Pergamon

Electrochimica Acta, Vol. 43, No. 24, pp. 3693–3701, 1998

Printed in Great Britain

PII: S0013-4686(98)00127-3

0013–4686/98 $19.00 + 0.00

Effects of Nafion impregnation on performances of PEMFC electrodes

S. J. Lee,[a]* S. Mukerjee,[a] J. McBreen,[a] Y. W. Rho,[b] Y. T. Kho[b] and T. H. Lee[c]

[a]Department of Applied Science, Brookhaven National Laboratory, Building 480, Upton, NY 11973, U.S.A.

[b]R&D Center, KOGAS, Ansan, Il-Dong, Kyunggi-Do, Korea

[c]Department of Chemical Engineering, Yonsei University, Seoul, Korea

(Received 20 December 1997; in revised form 20 December 1997)

Abstract—The effect of Nafion loading on the electrode polarization characteristics of a conventional proton exchange membrane (PEM) fuel cell electrode has been investigated in terms of both H_2/O_2 and H_2/air performance. Correlation of Nafion loading with the activation polarization characteristics shows an initial increase of activity upto a loading of 1.3 mg/cm^2 followed by a more gradual change with maxima at 1.9 mg/cm^2 for both oxygen and air. This trend correlated well with the decrease in charge transfer resistance and increase in the electrochemically active surface area. The contributions to the linear ohmic polarization region of both the H_2/O_2 and H_2/air performance are predominantly from ionic resistance as well as diffusional contributions in the catalyst layer. Among all the polarization losses those due to mass transport were the highest. Fits using a thin film agglomerate model showed a rapid increase in the film thickness with Nafion loading in the pores of the carbon of the catalyst layer followed by an equilibrium of ~800 Å thickness at a Nafion loading of 1.9 mg/cm^2. Further additions caused deeper penetration of this Nafion film into the catalyst layer increasing the diffusional pathways for the reactant gases. These results correlate well with the mass transport characteristics in O_2 and air as well as morphological characterization of the electrode based on SEM and pore volume distributions.

Key words: proton exchange membrane fuel cell, Nafion loading, active surface area, mass transport.

INTRODUCTION

Proton exchange membrane (PEM) fuel cells have significant advantages such as the elimination of electrolyte leakage, lower corrosion, simplification of stack design and increased ruggedness. These promising attributes have stimulated applications in areas such as military, aerospace and transportation [1]. Despite the advantages, PEMFC has several drawbacks to overcome including high cost, high catalyst loading and low CO tolerance.

From the perspective of electrode performance, the cost problem can be tackled in two ways: reduction of the catalyst loading and improvement of the catalyst utilization and performance. Significant cost reduction by decreasing the catalyst loading has been reported [2–4]. The underlying concept of reducing catalyst loading is to enhance catalyst utilization in the gas diffusion electrode. It is worthwhile to note that only catalyst in contact with both membrane electrolyte and reaction gas is electrochemically active. This has been amply demonstrated previously [5–7] via impregnation of solubilized ionomers like Nafion into the gas diffusion electrode.

Previous reports by Poltarzewski *et al.* [8, 9] on the effect of Nafion loading have indicated that in double layer electrode structures (substrate + catalyst layer) the Nafion loading primarily affects the ionic resistance of the catalyst layer. These reports suggest that the initial Nafion loading fill up the pores of the catalyst layer, subsequent additions of the solubilized Nafion results in formation of films on the surface of the electrode. Since the ionic

*Author to whom correspondence should be addressed. Tel.: +1 516 344 7740; Fax: +1 516 344 4071; E-mail: sjlee@bnl480.das.bnl.gov

resistance of this film is higher than the Nafion membrane, this acts in increasing the overall ionic resistance of the electrode. Recent studies using perfluorinated sulfonate ionomer (PFSI) colloids [10, 11], to prepare catalyst layers in gas diffusion electrode for PEM fuel cells have shown the importance of the microstructure of the catalyst layer and the role of the gas supplying network. In these reports higher concentration of PFSI in the catalyst layer caused the larger pores (macro-pores), space between the agglomerates to fill up without effecting the smaller pores (micro-pores) associated with space in and between primary particles in the agglomerate. This existence of two distinctive pore size distributions in a gas diffusion electrode structure has been alluded to before by Watanabe *et al.* [12, 13]. Other reports [14–16], primarily on gas diffusion electrodes for phosphoric acid fuel cells, have also shown the importance of the morphological characteristics of the electrode in relation to its overall performance.

In this study, we investigate the effects of Nafion impregnation on commercial low platinum-loading PEM electrodes. The objective is to resolve the effect of Nafion loading in its effect in the various polarization regions, activation, ohmic and mass transport. For this purpose steady state polarization measurement in single cells were correlated with results of impedance and morphological characterization. The impedance measurements were used to obtain charge transfer resistance and ohmic behavior. The morphological characteristics included measurements of the macropore volume distribution and scanning electron microscopy (SEM).

EXPERIMENTAL

Electrodes and preparation of membrane/electrode assemblies

The electrodes used in the preparation of the membrane/electrode assembly were purchased from Globe Tech (Bryan, Texas). The electrode structure was akin to currently available commercial PEM electrodes. It comprised of a carbon cloth substrate of approximate thickness ~35 mm (non-wet proofed), with wet-proofed (30–40% PTFE) carbon layer (Vulcan XC 72, Cabot) on both sides of the substrate with an average thickness of 20–30 μm. The catalyst layer deposited on one side of this assembly had a PTFE loading of approximately (30–40% PTFE), with an average thickness of 30–35 μm. The electrocatalyst, a 20% Pt on carbon support (Vulcan XC 72), was diluted with carbon (Vulcan XC 72) to obtain an average Pt loading of 0.4 mg/cm^2 in the catalyst layer. Methodology used to prepare this electrode was based on a proprietary rolling technique. Prior to preparation of the membrane-electrode assembly, the electrodes were impregnated with different loading of solubilized Nafion (Aldrich Chemicals), which has a molecular weight of 1100 and an average aggregate size of 50 Å. This impregnation was achieved via a brushing technique described before [2, 6, 7]. The Nafion was allowed to diffuse into the electrode structure for 10 min after application, which was followed by drying in air for 2 h at 80°C to eliminate residual aliphatic alcohol. The amount of impregnated Nafion was varied from 0 to 2.7 mg/cm^2 (dry weight of Nafion).

The membrane electrode assembly was prepared with a Nafion 115 membrane (125 μm, DuPont) which was cleaned by immersing in boiling 3% H_2O_2 for 1 h and then in boiling 1 M H_2SO_4 for the same time. The membrane was then rinsed in boiling deionized water for 1 h and the procedure was repeated at least twice to remove the sulfuric acid completely. After completing the membrane and electrode treatment, they were assembled and hot pressed at 140°C, 1000 kg_f/cm^2 for 3 min.

Measurement of electrode polarization in PEMFC single cells

A single cell, with a 1 cm^2 geometric area for the membrane/electrode assembly, was used in this study. This provided the opportunity for conducting simultaneous steady state polarization measurements as well as impedance spectroscopy for the same membrane electrode assembly. For checking the reproducibility of the polarization data a limited number of tests were conducted using a 5 cm^2 single cell/membrane electrode assembly. The bipolar end plates (graphite) in the single cell had series parallel type ribbed channels for the distribution of reactant gases. This bipolar plate had arrangements for a built in reversible hydrogen electrode on the anode side. This enabled measurements of both single and half-cell polarization in the same fixture. Teflon-coated fiberglass gaskets were positioned in both sides of the exposed area of the membrane to prevent gas leakage and membrane dryness. Current collecting copper plates were attached behind the graphite blocks.

The single cell was installed in a fuel cell test station equipped with provisions for temperature and pressure control, humidification of reactant gases and flow control (mass flow). The performance determination of the single cell was carried out using a personal computer and an electronic load (HP-6050A, Hewlett Packard Co.) interfaced through GPIB (general purpose interface board) and a data acquisition/control software written in-house. In order to maintain high ionic conductivity of the membrane, the reactant gases were humidified at 10°C higher than the cell. The gas flow rate was changed with current in order to keep a constant stoichiometry (2 × stoichiometric). Cell potential vs current density measurements were conducted using H_2/O_2, H_2/air over a pressure range of 1 to 2 atm at 70°C.

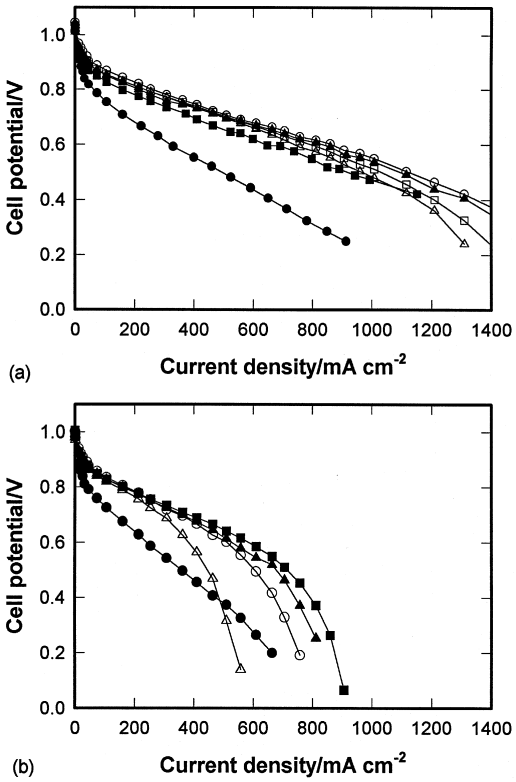

Fig. 1. Cell potential vs current density plots at 70°C, 2 atm for (a) H_2/O_2 and (b) H_2/air, as a function of Nafion loading. (●) 0.0, (■) 0.6, (▲) 1.3, (○) 1.9, (□) 2.1 and (△) 2.7 mg/cm^2.

Electrochemical characterization

An impedance analyzer (IM5d, Zahner Elektrik) measured the resistance of the membrane/electrode assemblies (1 cm^2 geometric area) at 0.9 V under operating cell conditions. The reference and counter electrode were connected to the hydrogen electrode and the working electrode was linked to the oxygen electrode. The current responses with respect to the 10 mV sine wave were evaluated in the frequency range of 50 mHz to 5 kHz.

Cyclic voltammetry measurements were conducted at 70°C on both 1 and 5 cm^2 geometric area single cell fixtures to determine the electrochemically active surface area (data for a 5 cm^2 electrode is used in this paper). The measurements involved hydrogen and N_2 at the counter electrode (anode) and working electrodes (cathode), respectively, with a potential range of 0.1 to 1.2 V vs RHE and a sweep rate of 20 mV/s. The electrochemically active surface area of the electrode was obtained from the charge required for hydrogen desorption from the Pt electrocatalyst. The coloumbic charge for the oxidation of atomic hydrogen (area under the anodic peak minus the double layer charge at 0.4 V vs RHE) was used to evaluate the roughness factor of the electrode assuming a value of 220 μC/cm^2 for the oxidation of atomic hydrogen on smooth Pt surface.

Morphological characteristics measurements

The morphological characterization of the electrodes was carried out using a SEM (5410LV, JEOL) and BET surface analyzer (ASAP 2400, Micrometrics). The SEM and BET surface analyzer provided surface structure and pore volume distribution of the electrode, respectively. The pore volume distribution was determined using the BJH principle determined according to the methodologies derived earlier [17].

RESULTS AND DISCUSSION

Electrochemical studies

Figure 1(a)–(b) shows the single cell performance of H_2/O_2, H_2/air showing the effect of Nafion loading on the electrode polarization characteristics at 2 atm pressure. From an overall performance point of view, the optimum Nafion loading for the H_2/O_2 was 1.9 mg/cm^2 and the corresponding value for H_2/air was 0.6 mg/cm^2, a considerably lower value. In order to understand the true significance of the effect of Nafion loading on the electrode performance it is necessary to examine its effect in all the three polarization regions corresponding to the activation, ohmic and mass transport. The activation (Tafel kinetic parameters) and ohmic polarization characteristics of the half cell polarization until the end of the linear region in the single cell, potential, E, vs current density, i, data correspond to the equation:

$$E = E_o - b \log i - Ri \quad (1)$$

where

$$E_o = E_r + b \log i_o \quad (2)$$

In these equations, i_o is the exchange current density for oxygen reduction, b is the Tafel slope, E_r is the reversible potential for the oxygen electrode reaction and R is predominantly the ohmic resistance in the electrode and electrolyte responsible for the linear variation of the potential vs current density plot. The parameters E_o, b and R were evaluated by a non-linear least-square fit of equation (1) to the experimental data (Table 1) for both H_2/O_2 (1 and 2 atm) and H_2/air (2 atm) pressure. There is a significant change in the electrode kinetics such as current density at 900 mV ($i_{900\ mV}$) for Nafion loading in the range, 0 to ~1.3 mg/cm^2 for H_2/O_2 and H_2/air, further application of Nafion caused relatively smaller changes. These are shown in a representative plot at 2 atm pressure for H_2/O_2 and H_2/air in terms of variation on $i_{900\ mV}$ as a function of Nafion loading (Fig. 2). An examination of the iR corrected Tafel plot (Fig. 3) at 2 atm pressure shows that the biggest variation in the plots occurs

Table 1.
Electrode kinetic parameters for oxygen reduction in PEMFC at 70°C and 2 atm pressure, using 0.4 mg/cm^2 Pt loading electrodes with various Nafion loading

Nafion loading (mg/cm^2)	Oxidant	Pressure (atm)	E_0 (mV)	b (mV/decade)	R (Ω cm^2)	$i_{900\ mV}$ (mA/cm^2)	Active surface area (cm^2/cm^2)	Charge transfer resistance (Ω cm^2)
0	oxygen	1	985	107.8	0.485	10.3	10.8	1.770
		2	1017	100.9	0.509	15.5		
	air	2	973	78.3	0.787	10.2		
0.6	oxygen	1	988	61.5	0.356	20.4	61.5	0.458
		2	1018	78.5	0.315	30.2		
	air	2	996	64.5	0.334	24.7		
1.3	oxygen	1	997	61.5	0.331	26.7	89.6	0.380
		2	1025	63.4	0.310	43.4		
	air	2	996	64.4	0.335	28.2		
1.9	oxygen	1	1008	61.3	0.320	37.5	115.0	0.307
		2	1032	59.9	0.312	50.3		
	air	2	997	56.4	0.423	32.2		
2.1	oxygen	1	994	62.0	0.310	25.5	127.4	0.445
		2	1018	63.6	0.288	42.0		
	air	2	–	–	–	–		
2.7	oxygen	1	989	64.9	0.333	21.1	133.6	0.450
		2	1014	62.5	0.297	35.5		
	air	2	973	78.3	0.787	22.5		

on the initial addition of Nafion (0.0 to 0.6 mg/cm^2). Besides transition towards higher potentials, the Tafel slope changes from 120 to 60 mV/decade indicating a strong influence of active surface area and those due to charge transfer and internal ionic resistance. This is expected since application of Nafion to an electrode surface is expected to increase the three-phase activation zone comprising of reactant gas, electrolyte and electrocatalyst.

The electrochemically active surface area of the electrode was measured by cyclic voltammograms. The coulombic charge for oxidation of the adsorbed atomic hydrogen (area under the anodic peak minus the double layer charge), assuming a coulombic charge of 220 μC/cm^2 for the oxidation of absorbed atomic hydrogen on smooth Pt was used (Fig. 4 and Table 1). The charge transfer resistance was obtained using impedance analysis (Fig. 5) as a function of Nafion loading in a single cell with H_2/O_2 flow at 0.9 V at 2 atm pressure. The charge transfer resistance delineated as Nyquist plots shows a four-fold change in going from 0 to 1.3 mg/cm^2 Nafion loading. Beyond 1.3 mg/cm^2, the

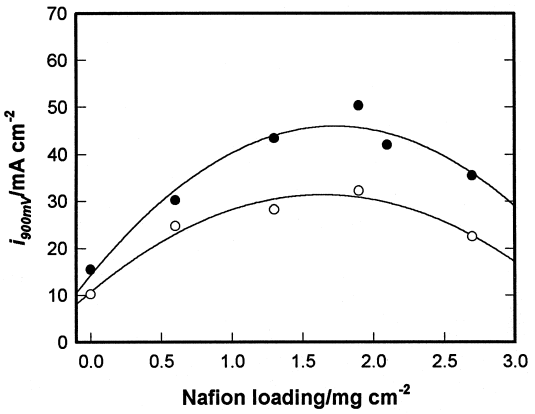

Fig. 2. Variation of current density at 900 mV ($i_{900\ mV}$) for H_2/O_2 (●) and H_2/air (○) at 70°C, 2 atm as a function of Nafion loading.

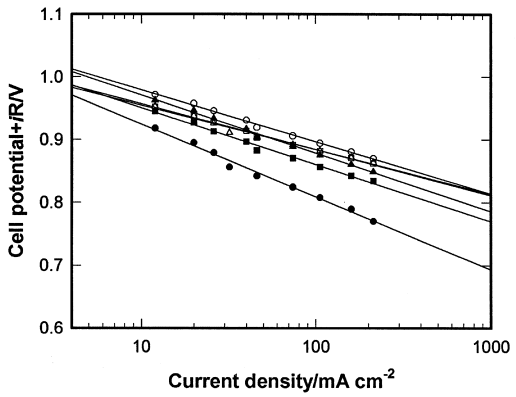

Fig. 3. *iR* corrected Tafel plots for oxygen reduction at 70°C, 2 atm as a function of Nafion loading. (●) 0.0, (■) 0.6, (▲) 1.3, (○) 1.9, (□) 2.1 and (△) 2.7 mg/cm^2.

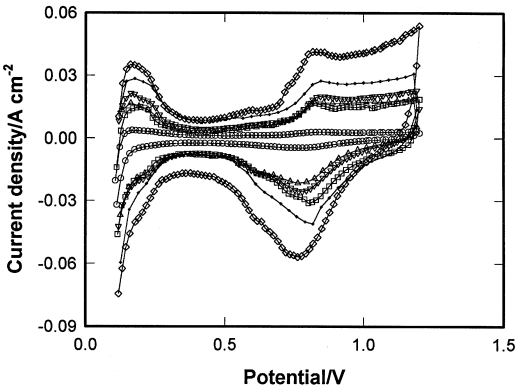

Fig. 4. Cyclic voltammograms at 70°C and 1 atm as a function of Nafion loading (scan rate: 20 mV/s). (○) 0.0, (□) 0.6, (△) 1.3, (▽) 1.9, (+) 2.1 and (◇) 2.7 mg/cm^2.

change is more gradual, with the lowest value (0.307 Ω cm^2) obtained at a Nafion loading of 1.9 cm^2. This increase in the electrochemically active surface area and decrease in the charge transfer and internal ionic resistance correlate well with the Tafel kinetic parameters in the activation controlled region (Fig. 6). Both these parameters show a rapid change in magnitude from 0 to 1.3 mg/cm^2 followed by a more gradual variation. In other words, increase in the Nafion content results in the extension of the reaction zone (active area) and a consequent decrease in the charge transfer and internal ionic resistance resulting in improved activation polarization characteristics.

The ohmic polarization losses obtained from the non-linear least-square fit of equation (1) in the linear part of the E vs i variation (such as those shown in Fig. 1) shows the biggest change in going from 0 to 0.6 mg/cm^2 Nafion loading for both H_2/O_2 and H_2/air. This measured resistance is the sum total of all resistance in the electrode/membrane electrolyte interface which includes membrane resistance, some contribution of ionic resistance of the electrolyte in the reaction layer, contact resistance in the single cell, hydrogen polarization losses and some contributions from the mass transport. However the contribution of the membrane resistance determined via impedance measurement was

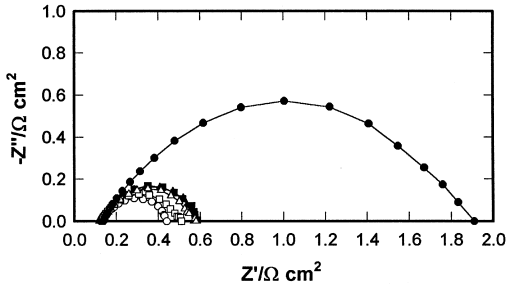

Fig. 5. Complex impedance behavior using H_2/O_2 at 0.9 V as a function of Nafion loading. (●) 0.0, (■) 0.6, (▲) 1.3, (○) 1.9, (□) 2.1 and (△) 2.7 mg/cm^2.

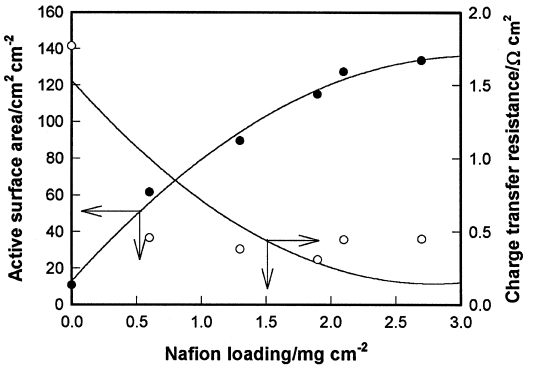

Fig. 6. Variation of electrochemically active surface area (●) and charge transfer resistance (○) as a function of Nafion loading.

constant as shown in the high frequency region of Fig. 5. In addition, the contributions due to contact resistance and hydrogen electrode polarization are expected to remain constant as a function of Nafion loading. Hence the major contributor to the variation in the magnitude of R (Fig. 7) is the combination of ionic resistance and mass transport in the reaction layer.

Figure 1(b) shows the influence of Nafion loading on cell performance when the oxidant is air. A Nafion loading above 0.6 mg/cm^2 caused a decrease in cell performance (limiting currents) at higher current densities (mass transport region). The corresponding H_2/O_2 performance [Fig. 1(a)] shows a different optimum loading of 1.9 mg/cm^2. These mass transport limitations are a direct function of diffusional resistance in the catalyst layer causing hindrance to access by oxygen to the active agglomerates.

This suggests that while the activation polarization and the ohmic losses in the cell show small variations as a function of Nafion loading beyond 0.6 mg/cm^2, the principal role in determining the overall cell performance appears to be related to

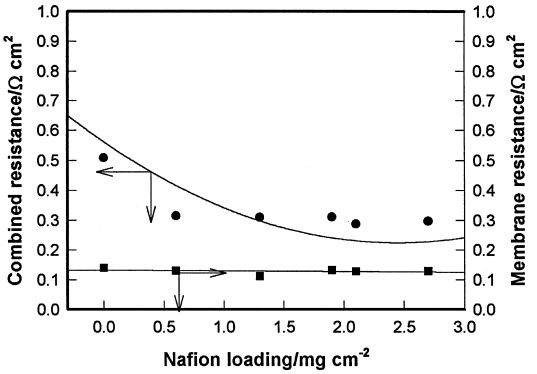

Fig. 7. Effect of Nafion loading on membrane resistance (■), derived from high frequency impedance behavior and combined resistance (●) determined from Tafel behavior at 70°C, 2 atm.

mass transport. This is especially apparent for the H_2/air single cell performance.

The total surface area of Pt in the catalyst layer, based on an average particle size of 35 Å [18] and a cubo-octahedron cluster model provides for 1415 atoms to a cluster, hence 2.18×10^{18} clusters/gm, corresponding to total surface area of 88.7 m^2/gm. Based on a Pt loading of 0.4 mg/cm^2 in the electrode, we get a roughness factor of 355 cm^2/cm^2. This value compares well with calculations based on the density of Pt using the equation $A/g = 3/r\rho$ giving a roughness factor of 320 cm^2/cm^2. Comparison of the ratio of the actual electrochemically active surface area measured from cyclic voltammogram (Table 1) and the total surface area (based on 35 Å particle size) as a function of Nafion loading shows a steady increase. This indicates steadily deeper impregnation of Nafion into the catalyst layer. Taking the density of hydrated Nafion as 1.58 g/cm^3 [19] and a Nafion loading of 1.9 mg/cm^2 results in a Nafion volume of 1.25×10^{-3} cm^3/cm^2 in the catalyst layer. With 20% Pt loading on carbon we have 1.6 mg/cm^2 carbon loading and hence a volume contribution of 1×10^{-3} cm^3/cm^2 (taking the density of carbon as 1.6 g/cm^3). Assuming 70% void volume in the carbon we have a void volume of 3.3×10^{-4} cm^3/cm^2. Hence, at a Nafion loading of 1.9 mg/cm^2 when approximately a third of the Pt is electrochemically active the Nafion forms a discrete film occupying ~third of the catalyst layer.

A simplified model based on the original flooded agglomerate approach by Giner and Hunter [20] and later developed by Cutlip and Iczkowski [21] has been extended to include the thin film diffusion process in a PEM environment by Springer and Raistrik [22]. In this model the electrode structure is considered to be a dual-scale macro–microporous interconnected region with the hydrophobic regions allowing reactant gas access to the surface of all agglomerate regions. The agglomerate is considered as those consisting of interconnected regions of catalyst containing carbon and electrolyte. The agglomerate region is separated from the hydrophobic gas channels by a thin film of electrolyte. Hence the concentration profile of the reactant gas in this layer is considered to vary in a non-linear fashion since the electrochemical reaction at any point is dependent to the local reactant concentration [22]. This model shows that as in the case of internal resistance effect, when the diffusion of oxygen in the agglomerate controls the reaction kinetics, a doubling of the Tafel slope in the *iR* corrected Tafel plot is expected. However, variation of the Tafel slope with the Nafion loading reaches an equilibrium (Table 1) value beyond 0.6 mg/cm^2. This therefore points to the absence of diffusional problems within the agglomerate. Hence, the principal diffusional contribution in the mass transport is expected to be due to the thin film around the agglomerate.

Using the derived expression based on this model for our discussion on the contribution of the Nafion film thickness on the mass transport characteristics we have:

$$j = \frac{e^{\mu}}{1 + \Gamma e^{\mu}} \tag{3}$$

where j is the reduced current density ($j = i/i_o$), μ is the reduced overpotential (η/b) and Γ is the film diffusion parameter. The thin film diffusion parameter is defined as $\Gamma = \kappa^o \delta / D_f$, where κ^o is the effective rate constant at reversible potential, δ is the film thickness (cm) and D_f is the diffusion coefficient of oxygen in the thin film (cm^2/s). The effective rate constant κ^o is related to the rate constant of the catalyst at reversible potential κ', catalyst area per unit volume A_v (cm^{-1}) and thickness of the agglomerate region L_y (cm) by the expression $\kappa^o = \kappa' A_v L_y$ (cm/s). Simplifying equation (3) we have:

$$b \log\left(\frac{i}{i_o - i\Gamma}\right) = \eta \tag{4}$$

Non-linear least square fitting of the current (i) and iR corrected overpotential (η) for H_2/O_2 performance at 2 atm pressure was used for determining the values of Γ, i_o and b as a function of Nafion loading (Fig. 8). equation (3), when used in conjunction with iR corrected overpotential, reduces to $j = e^{\mu}$ for the reduced current density (activation

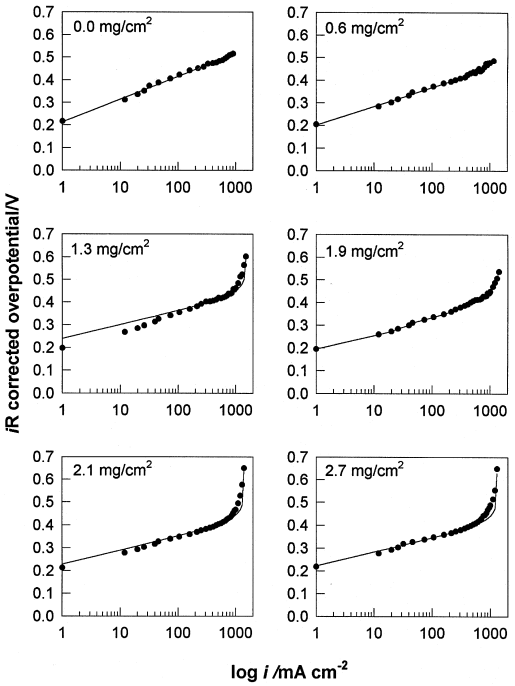

Fig. 8. Fits of experimental results based on iR corrected overpotential vs. log i (•) and those calculated from thin film agglomerate model (———) as a function of Nafion loading.

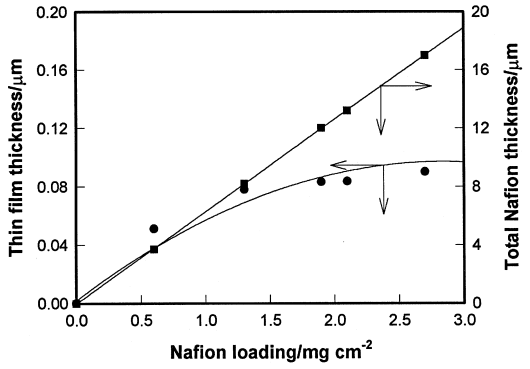

Fig. 9. Variation of thin film thickness (●), derived from thin film agglomerate model and total Nafion film thickness (■) assuming zero Nafion penetration in catalyst layer as a function of Nafion loading.

controlled region) from a flat electrode surface with no mass transport limitation. Hence, equations (3) and (4) when used in conjunction with iR corrected overpotential (η) follows the entire electrode polarization behavior assuming that the major contributor to the mass transport is the diffusion through the thin film. Representative fits shown for H_2/O_2 at 2 atm pressure show that this assumption is true based an average value of ~95% for the confidence of fit.

The values of Γ obtained from this treatment was used for calculating the thin film thickness, δ using the expression [22]:

$$\delta = \frac{nFC^*D_f\Gamma}{i_o} \tag{5}$$

derived from equations, $\Gamma = \kappa^o\delta/D_f$ and $i_o = nFC^*\kappa^o$, where C^* is the reactant concentration in the bulk electrolyte (mol/cm^3). The values of δ (μm) thus obtained are plotted as a function of Nafion loading in Fig. 9. The trend follows a pattern showing an initial increase in the film thickness followed by attainment of an equilibrium thickness at ~1.9 mg/cm^2. Since the active area keeps increasing it appears that further increase in the Nafion loading results in deeper penetration of the Nafion into the catalyst layer without increasing the film thickness. This is also apparent from the comparison with the total Nafion film thickness (calculated using $l = m/A\rho$) assuming zero penetration into the catalyst layer (Fig. 9) which shows a linear increase with Nafion loading. Hence the mass transport contributions are primarily due to formation of Nafion films, first with increasing thickness and then with increasing lengths over the gas channels in the catalyst layer. In order to confirm this, morphological characterization of the electrode was carried out using pore volume distribution measurements and scanning electron microscopy.

Correlation of electrochemical and morphological characteristics

Figure 10 shows the top-view SEM images of the Pt/C electrodes with various Nafion loadings. Figure 11 shows the pore volume distribution in the catalyst layer as a function of Nafion loading obtained with a BET surface analyzer. In Fig. 10 it is seen that for the electrode without Nafion, there appear to be lots of pores, which serve as macroporous channels for gas flow [Fig. 10(a)]. However, with increasing Nafion loading, the majority of the front surface pores gradually get covered by impregnated Nafion [Fig. 10(b)–(f)].

This is further confirmed for the inner pores by the macropore volume distribution (Fig. 11). As the Nafion loading is increased, the number of pores with the diameter in the range of 100 to 1000 Å is reduced, indicating blockage by Nafion. These results also show that for higher Nafion loading the pore volume distribution range is narrowed. In addition, above a Nafion loading of 1.9 mg/cm^2, the pore volume distribution appears to reach equilibrium.

Discussion

Differences with previous results by Poltarzewski *et al.*, [8, 9] which suggest the formation of Nafion film on the front surface of the electrode is related to (a) differences in the electrode structure and (b) to the methodology of Nafion impregnation. The electrode structures used by Poltarzewski were based on wet proofed carbon paper backing instead of the carbon cloth more commonly used in PEM electrodes. Further, there was no wet proofed carbon layer on both sides of the carbon paper substrate in contrast to the electrode used in this investigation. Nafion was impregnated by floating the electrode on the solubilized Nafion solution instead of a brushing technique used in this investigation. Due to these differences the optimum Nafion loading was different and there was no film formation on the front surface of the reaction layer in our electrode. However there is agreement on the fact that diffusional resistance due to Nafion film formation is the primary cause of performance losses at Nafion loading beyond the optimum value. The results of this study also agree with recent reports on new electrode structures using colloidal mixtures of perfluorinated sulfonic acid ionomers (PFSI) together with the Pt/C and PTFE/C as a reaction layer [10, 11]. In these reports formation of thin film of Nafion on agglomerates is reported to be the primary source of diffusional resistance. It was shown that larger pores >400 Å decreased with an increase of the PFSI content in similar lines to our report. Further this report also showed that the Nafion film formation in the larger pores were the primary source of diffusional losses.

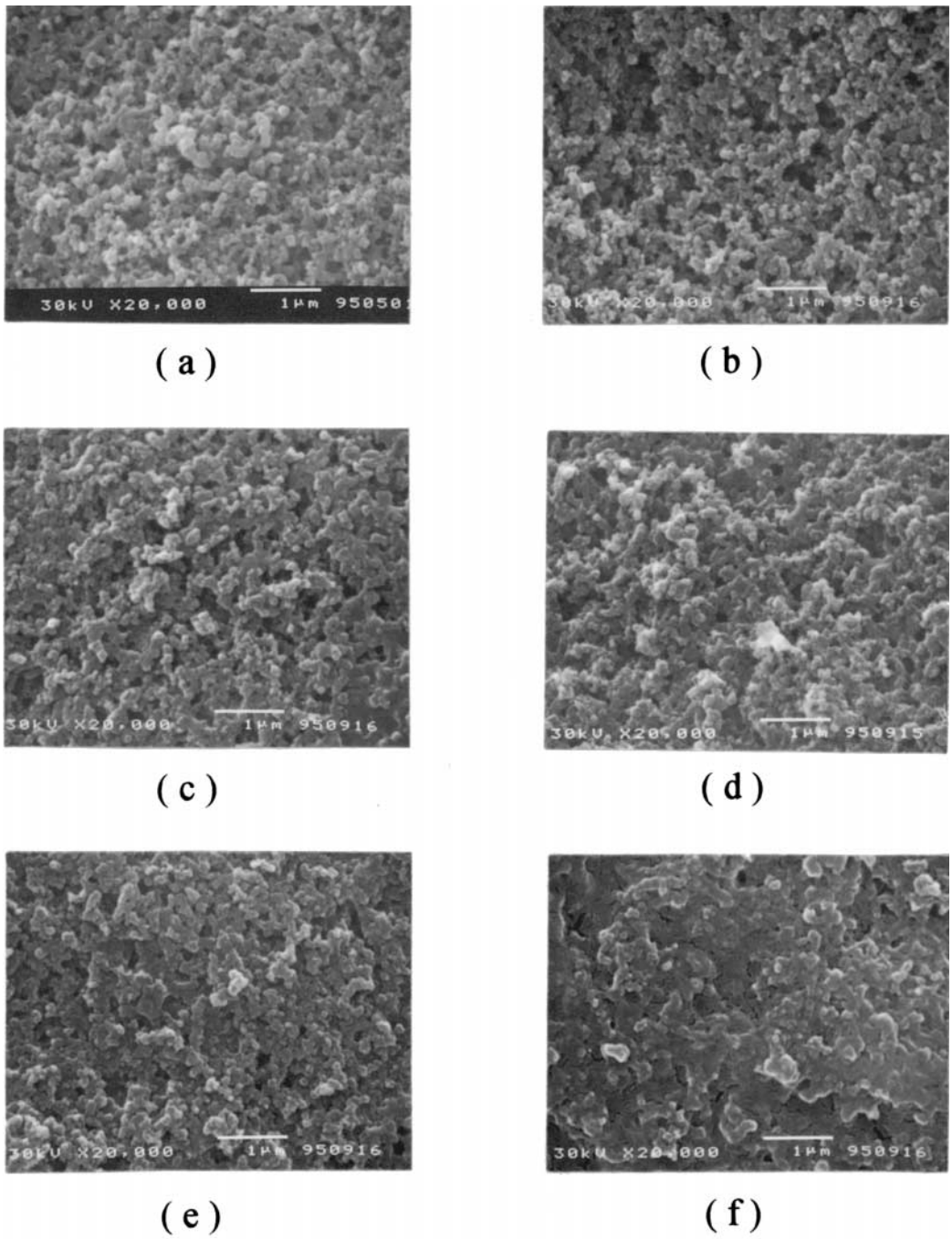

Fig. 10. SEM photographs of the electrodes with various Nafion loading (a) 0, (b) 0.6, (c) 1.3, (d) 1.9, (e) 2.1 and (f) 2.7 mg/cm^2.

CONCLUSIONS

The effect of Nafion loading on the electrode polarization behavior has been investigated for a conventional low Pt loading (0.4 mg/cm^2) PEM fuel cell electrode. In the low current density region (activation polarization), the primary effect of Nafion addition is the lowering of the charge transfer resistance resulting in reduction of the Tafel slope from 120 to 60 mV/decade and the increase in the electrochemically active surface area. The effect in terms of electrode kinetic parameters such as $i_{900\ \mathrm{mV}}$ is a rapid increase in activity followed by a more gradual change beyond $\sim$1.3 mg/cm^2 Nafion loading, trends similar to the variation of electrochemically active surface area. The main contributor to the linear variations in the ohmic polarization region was due to ionic resistance and diffusional resistance indicating effects of increased thin film

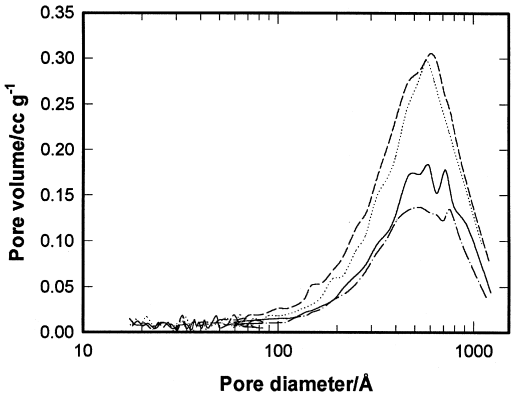

Fig. 11. Pore volume distribution of the catalyst layer, obtained from nitrogen desorption measured in a BET apparatus using the BJH approach, as a function of Nafion loading. (- - -) 0.0, (. . .) 0.6, (———) 1.9 and (– · –) 2.7 mg/cm^2.

thickness around the agglomerates. Among the three contributors (activation, ohmic and mass transport) to the overall polarization losses, mass transport losses were of the highest significance. Fits of the iR corrected current density to the overpotential η to a thin film/agglomerate model showed good fits in the mass transport region. This indicated that the diffusional resistance due to increased thin film thickness and higher penetration of the Nafion into the catalyst layer were the main contributor to the mass transport characteristics. This was particularly true for the H_2/air performance. Higher Nafion loading (beyond 1.9 mg/cm^2 for H_2/O_2 and 0.6 mg/cm^2 for H_2/air) indicated losses in macropore volume, necessary for high current density operation.

Comparison of the variation of the film thickness with the Nafion loading indicated the formation of an equilibrium film of ~800 Å at a Nafion loading of 1.9 mg/cm^2. A further increase in the Nafion loading caused an increase in the penetration depth of this film into the catalyst layer. This picture was in good agreement with the H_2/O_2 performance characteristics in the mass transport region in terms of the agreement of the maxima attained at 1.9 mg/cm^2. The lower optimum Nafion loading in the H_2/air performance was a result of lower oxidant concentrations, C^*, at the interface. Normalization of the concentrations with respect to that for air at 2 atm pressure provided good agreement with the agglomerate thin film model description. This model was further confirmed using both SEM and the pore volume distribution measurements.

ACKNOWLEDGEMENTS

The authors acknowledge the support of the U.S. Department of Energy under Contract No. DEA-CO2-76CH00016 and the Korea Science and Engineering Foundation under Contract No. 93-0600-01-01-3. S. J. L. was supported by a 1996 Abroad Post-Doc. Program from Ministry of Education of Korea. The authors also express their deep appreciation to Dr Edson Ticianelli for his advise and help in data analysis and preparation of this manuscript.

REFERENCES

1. H. P. Dhar, *J. Electroanal. Chem.* **357,** 237 (1993).
2. E. A. Ticianelli, C. R. Derouin and S. Srinivasan, *J. Electroanal. Chem.* **251,** 275 (1988).
3. M. S. Wilson and S. Gottesfeld, *J. Electrochem. Soc.* **139,** L284 (1992).
4. E. J. Taylor, E. B. Anderson and N. R. K. Vilambi, *J. Electrochem. Soc.* **139,** L45 (1992).
5. I. D. Raistrick, U.S. Patent, 4, 876115, 1990.
6. E. A. Ticianelli, C. R. Derouin, A. Redondo and S. Srinivasan, *J. Electrochem. Soc.* **135,** 2209 (1988).
7. K. Petrov, K. Xiao, E. R Gonzalez, S. J. Srinivasan, A. J. Appelby and O. J. Murphy, *Int. J. Hydrogen Energy* **18,** 907 (1993).
8. Z. Poltarzewski, P. Staiti, A. Alderucci, W. Wieczorek and N. Giordano, *J. Electrochem. Soc.* **139,** 761 (1992).
9. P. Staiti, Z. Poltarzewski, A. Alderucci, G. Maggio and N. Giordano, *Int. J. Hydrogen Energy*. **19,** 523 (1994).
10. M. Uchida, Y. Aoyama, N. Eda and A. Ohta, *J. Electrochem. Soc.* **142,** 463 (1995).
11. M. Uchida, Y. Aoyama, N. Eda and A. Ohta, *J. Electrochem. Soc.* **142,** 4143 (1995).
12. M. Watanabe, M. Tomikawa and S. Motoo, *J. Electroanal. Chem.* **195,** 81 (1985).
13. M. Watanabe, K. Makita, H. Usami and S. Motoo, *J. Electroanal. Chem.* **197,** 195 (1986).
14. N. Giordano, E. Passalacqua, V. Alderucci, P. Staiti, L. Pino, H. Mirzaiani, E. J. Taylor and G. Wilemski, *J. Electrochim. Acta* **36,** 1049 (1991).
15. D. S. Chan and C. C. Wan, *J. Power Sources* **50,** 261 (1994).
16. T. Mori, J. Imahashi, T. Kamo, K. Tamura and Y. Hishinuma, *J. Electrochem. Soc.* **133,** 896 (1986).
17. E. P. Barrett, L. G. Joyner and P. P. Halenda, *J. Am. Chem. Soc.* **73,** 373 (1951).
18. S. Mukerjee and J. McBreen, *J. Electroanal. Chem.* (in press).
19. L. A. Zook and J. Leddy, *J. Anal. Chem.* **68,** 3793 (1996).
20. J. Giner and C. Hunter, *J. Electrochem. Soc.* **116,** 1124 (1969).
21. R. P. Iczkowski and M. B. Cutlip, *J. Electrochem. Soc.* **127,** 1433 (1980).
22. T. E. Springer and I. D. Raistrik, *J. Electrochem. Soc.* **136,** 1594 (1989).